INTERFACIAL PHENOMENA ON SELECTED CATHODE MATERIALS

Robert Kostecki, Yoshiaki Matsuo, Frank McLarnon
Lawrence Berkeley National Laboratory
Berkeley, CA 94720, USA

Abstract

We have carried out a series of surface studies of selected cathode materials. Instrumental techniques such as Raman microscopy, surface enhanced Raman spectroscopy (SERS), and atomic force microscopy were used to investigate the cathode surfaces. The goal of this study was to identify detrimental processes which occur at the electrode/electrolyte interface and can lead to electrode degradation and failure during cycling and/or storage at elevated temperatures

INTRODUCTION

(i) The $LiMn_2O_4$ spinel is of great interest as a cathode material for rechargeable lithium-ion cells because of its low cost and small environmental impact. However, it has been reported [1-20] that this material exhibits significant capacity fading during cycling or storage at elevated temperatures, which prevents its commercial use. Several mechanisms of capacity fading have been proposed, and it appears that the most important one is Mn dissolution [3-16]. It may occur via a disproportionation reaction of unstable Mn^{3+} to Mn^{2+} and Mn^{4+} in the presence of acid impurities or solvent oxidation products at high electrode potentials [6,8]. Manganese ion substitution by two Li^+ ions and formation of $Li_{1+2y}Mn_{2-y}O_4$ was also proposed as a possible mechanism of $LiMn_2O_4$ decomposition. It was also reported that observed capacity fading exceeded that calculated from the amount of dissolved Mn due to increased lattice disorder in the $LiMn_2O_4$ structure after storage in the electrolyte at 55°C [18].

In our earlier work [17], we also observed delithiation of thin-film $Li_2Mn_4O_9$ electrode in EC:DMC (1:1 by volume) 1M $LiPF_6$ electrolyte. Raman measurements showed clearly spontaneous conversion of the original material into λ–MnO_2 which was covered by a thin non-conductive layer, most likely Li_2O. However, we couldn't detect intercalated protons in this compound

In this study, we sought to characterize the SEI layer formation process on the $LiMn_2O_4$ electrode at elevated temperatures. To eliminate possible side reactions we prepared thin-film $LiMn_2O_4$ spinel electrodes with no additives. The $LiMn_2O_4$ electrodes were exposed to pure dimethyl carbonate (DMC) or to a standard 1M $LiPF_6$ - EC:DMC (1:1 by vol) electrolyte where EC = ethylene carbonate, DMC = di-methyl carbonate, at 55, 60 and 70°C. Surface reactions and their products were investigated by current-sensing atomic microscopy (CSAFM), Raman spectroscopy and surface enhanced Raman spectroscopy (SERS).

(ii) A baseline Li-ion cell defined by the DOE Advanced Technology Development (ATD) Program consists of a carbon anode (negative electrode), a $LiNi_{0.8}Co_{0.2}O_2$ cathode (positive electrode) and DEC-EC-$LiPF_6$ electrolyte. Nine ATD baseline cells were fabricated by PolyStor, Inc. according to a design provided by Argonne National Laboratory (ANL) and tested at Idaho National Engineering and Environmental Laboratory (INEEL), ANL and Sandia National Laboratories (SNL). These cells were not optimized, and were used only in studies of cell components under high-power battery simulations.

High-current pulse profiles were generated specifically for performance characterization of these batteries in the hybrid electric vehicle applications in contrast to the constant-current profiles typically used in the characterization of lithium-ion batteries in portable devices. Nine 18650-size ATD cells were tested under a variety of conditions. All cells had undergone two formation cycles and one discharge, and some were placed on calendar-life tests (the cells were stored at various temperature) or cycle-life tests (the cell was subjected to a charge-neutral profile with 3, 6, or 9% variation of its state of charge) [21]. The power performance (W/kg) of all cells decayed by 15-30% during cycle-life and calendar-life testing. The cells were then discharged at the C/25 rate and stored at 10°C. Cells were opened in a helium-atmosphere dry box, followed immediately by diagnostics.

In this paper we report results of diagnostic studies to characterize the cathodes taken from these cells. The goal of this study was to detect and characterize interfacial processes which occurred at the cathode/electrolyte interface and to determine their effect on the cathode electrochemical properties. Selected diagnostic techniques such as Raman spectroscopy, SERS, AFM and CSAFM were used to examine the surfaces of cathodes extracted from a fresh cell and cells after storage and cycle-life tests.

EXPERIMENTAL

(i) The thin-film $LiMn_2O_4$ electrodes were prepared by spin-coating of a homogeneous precursor solution onto a Pt substrate (about 1 cm^2), a procedure similar to that reported in our previous paper [17]. The average film thickness of 300 nm was estimated from ellipsometric mesurements. X-ray diffraction patterns and Raman spectra of the $LiMn_2O_4$ thin films confirmed a cubic spinel structure with a Fd3m space symmetry group and a 0.819 nm cubic cell lattice parameter.

Electrochemical measurements were carried out in a polypropylene beaker-type cell at room temperature or 55°C. Two separate pieces of Li foil were used as reference and counter electrodes. The electrolyte solution was commercial EC:DMC (1:1 by volume), 1 M $LiPF_6$ purchased from EM Science. DMC was obtained from Grant Chemical Division Ferro Corporation. Cyclic voltammograms (CVs) were recorded with a Model 362 EG&G scanning potentiostat at 1 mV/s. Thin-film $LiMn_2O_4$ electrodes were exposed to pure DMC or the -EC+DMC (1:1 by volume), 1 M $LiPF_6$ electrolyte at 60°C and 70°C for 1 day.

Ex-situ CSAFM images were obtained with a Molecular Imaging scanning probe microscope coupled with a Park Scientific Instruments (PSI) electronic controller.

Platinum-coated Si microlevers (0.12 Nm^{-1}) were used to probe the local electrode conductance. Conductance images were recorded at 1.0 V sample-tip bias i.e., the electrode was positive vs. the tip. The CSAFM experiments were carried out in N_2 atmosphere without exposing them to the air. Samples exposed to the electrolyte were rinsed with DMC and dried in N_2 gas stream.

Ex-situ Raman and SERS spectra were recorded using a Coherent Inc. Model Innova 70 Argon ion laser at λ=514.5 nm, an HR320 spectrograph (Instruments SA Inc.), and an EG&G multichannel analyzer Model 1463. The incident laser beam (0.1 x 3 mm) power measured at the sample was adjusted to 5 and 30 mW for SER and regular Raman measurements, respectively.

In order to obtain SER spectra of $LiMn_2O_4$ electrode after exposure to DMC or electrolyte solution, half of the electrode surface was coated with fine Ag particles. Silver AC sputtering was conducted at $5x10^{-2}$ bar vacuum, for 5s at relatively low current (40 mA). Raman and SER reference spectra of solid Li_2CO_3, CH_3COOLi, $NaHCO_3$, $(COONa)_2$ and HCOONa were obtained in a similar manner i.e., thin films of crystalline salts were partially coated with silver microparticles and then their regular Raman and SER spectra recorded at ambient conditions.

(ii) The 18650-size ATD cell characteristics are listed in Table 1 and a summary of the test conditions for all nine cells is given in Table 2. Detailed description of testing parameters and diagnostic experimental procedures can be found in [22].

Table 1 Generation 1 Cell Components

Component	Anode	Cathode
active material	75% MCMB graphite 17% SFG-6 carbon	84% $LiNi_{0.8}Co_{0.2}O_2$ Sumitomo
binder	8% polyvinylidene fluoride Kurecha C	8% polyvinylidene fluoride Kurecha 1100 (homopolymer)
additive	**NA**	4% acetylene black, Shawinigan 4% graphite, SFG-6
current collector	11 μm Cu foil	28 μm Al foil-uncoated
loading	5.5 mg/cm^2	10.2 mg/cm^2
separator	37 μm three-layer (PE/PP/PE) from Celgard	
electrolyte	1M $LiPF_6$ in EC/DEC (1:1), LP-40 from EM Science (Merck)	

Ex situ Raman spectra and CSAFM images were recorded using the instrumentation which was desribed in detaid in the above section.. AFM imaging was conducted in a small glove box specially designed for scanning-probe microscopy tests under a controlled N_2 atmosphere.

Table 2 Test conditions of the ATD GEN-1 cells

Cell number	SOC	Δ SOC	Temp (°C)	Testing period (weeks)
1	0	0	20	0
2	80	0	40	4
3	60	0	50	12
4	80	0	60	4
5	60	0	70	2
6	60	3	40	4
7	60	3	70	2
8	60	9	40	4
9	60	9	70	2

RESULTS

(i) Surface Layer Formation on a Thin-film $LiMn_2O_4$ Electrode

Figure 1 shows CVs of the fresh thin-film $LiMn_2O_4$ electrode and electrodes exposed to pure DMC (a), and the electrolyte solution (b), at 60°C and 70°C. Two anodic peaks at 4.05 and 4.17 V and two corresponding cathodic peaks at 4.03 and 3.90 V are characteristic for the $LiMn_2O_4$ spinel. The electrode exhibited moderate capacity loss of 0.2% per cycle over 43 cycles at room temperature.

A similar voltammetric curve was obtained for a $LiMn_2O_4$ electrode which was stored in pure DMC at 60°C for 1 day. Despite initially exhibiting 26% less capacity compared to the fresh $LiMn_2O_4$ electrode still showed good cycleability. However, storage of a $LiMn_2O_4$ electrode in pure DMC at 70°C led to its total deactivation. The fact that this degradation was not accompanied by even slight changes in its X-ray diffraction pattern suggests that the presence of a surface insulating layer is responsible for the observed loss of electrochemical activity.

Prolonged exposure of the $LiMn_2O_4$ electrode in the EC:DMC (1:1 by volume), 1 M $LiPF_6$ electrolyte led to irreversible destruction of the electrode. The higher the storage temperature, the greater the detrimental effect on the electrode

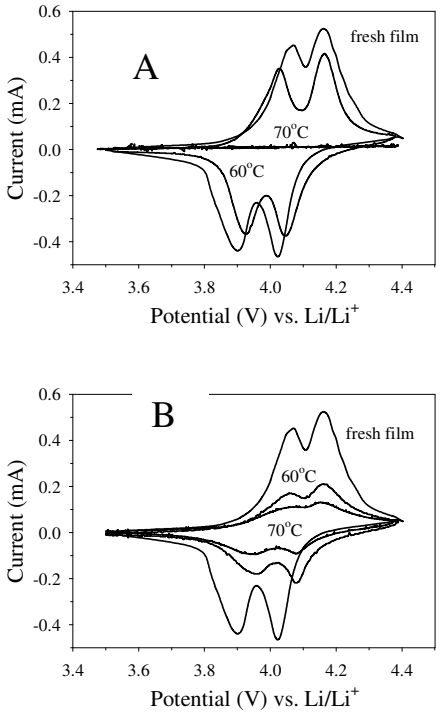

Figure 1. Cyclic voltammograms in 1M $LiPF_6$-EC+DMC (1:1 by volume) of a fresh thin-film $LiMn_2O_4$ electrode and those exposed to DMC (a) and to the electrolyte solution (b) for 1 day at 60°C and 70°C. Scan rate was 1 mV/s

capacity was observed. The electrode capacity dropped to 49% and 32% after storage at 60 and 70°C, respectively. Interestingly, the remaining active part of the electrode exhibited good cycleability and showed little capacity fading (3-4%) after 43 cycles. One can expect that DMC decomposition followed by formation of an insulating surface layer may contribute to the observed decline of electrode capacity in this case. However, the surface film must be either non-uniform or penetrable by the electrolyte because the electrode still shows some electrochemical activity.

Figure 2 shows topographic (upper) and conductance (lower) images of a fresh thin-film electrode. The electrode surface morphology consists of densely packed grains with the average roughness ca. 24 nm. The corresponding conductance image of the fresh $LiMn_2O_4$ electrode reveals non-uniform surface electronic conductivity. The brighter areas in the conductance images represent areas of relatively good conductivity whereas dark spots portray areas of poor conductivity. There are grains of active material which exhibit fairly good conductance, but we also found areas at the surface which show zero electronic conductivity. Interestingly, there are visible inhomogenities within single grains of $LiMn_2O_4$.

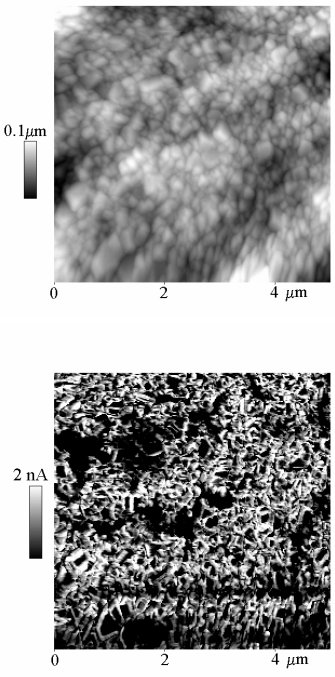

Figure 2. CSAFM topographic (upper) and conductance (lower) images of a fresh thin-film $LiMn_2O_4$ electrode. Bright areas on the conductance image represent high conductivity locations.

Figure 3 shows CSAFM images of $LiMn_2O_4$ electrodes exposed to pure DMC and the EC:DMC (1:1 by volume), 1 M $LiPF_6$ electrolyte at 60 and 70°C. Although the topographic image of the electrode exposed to pure DMC at 60°C appeared very similar to that of the fresh electrode, the surface conductance decreased substantially over the entire surface. The surface smoothing effect combined with surface electronic conductivity loss may suggest either formation of an insulating surface layer and/or surface conversion of the $LiMn_2O_4$ into a non-conducting compound. When the thin-film electrode was exposed to pure DMC at 70°C the observed surface effects became even more pronounced. The average surface roughness decreased to 9 nm and surface conductance dropped to zero over the entire electrode surface.

CSAFM images of the thin-film $LiMn_2O_4$ electrode exposed to the electrolyte solution at 60°C show evidence of severe damage to the film structure. Formation of round pits of ~1 μm dia. and ca. 150 - 250 nm deep was detected, a clear indication of manganese dissolution. Surface conductance also dropped significantly at most of the surface, however, conductive spots were still present. Similarly to pure DMC, storage in the electrolyte at 70°C resulted in the complete loss of surface conductance of the thin-film $LiMn_2O_4$ electrode. Examination of the corresponding topographic image reveals substantial changes in the electrode surface morphology and structural damage to the film. The size of pits grew larger to almost 2 μm in diameter but they became

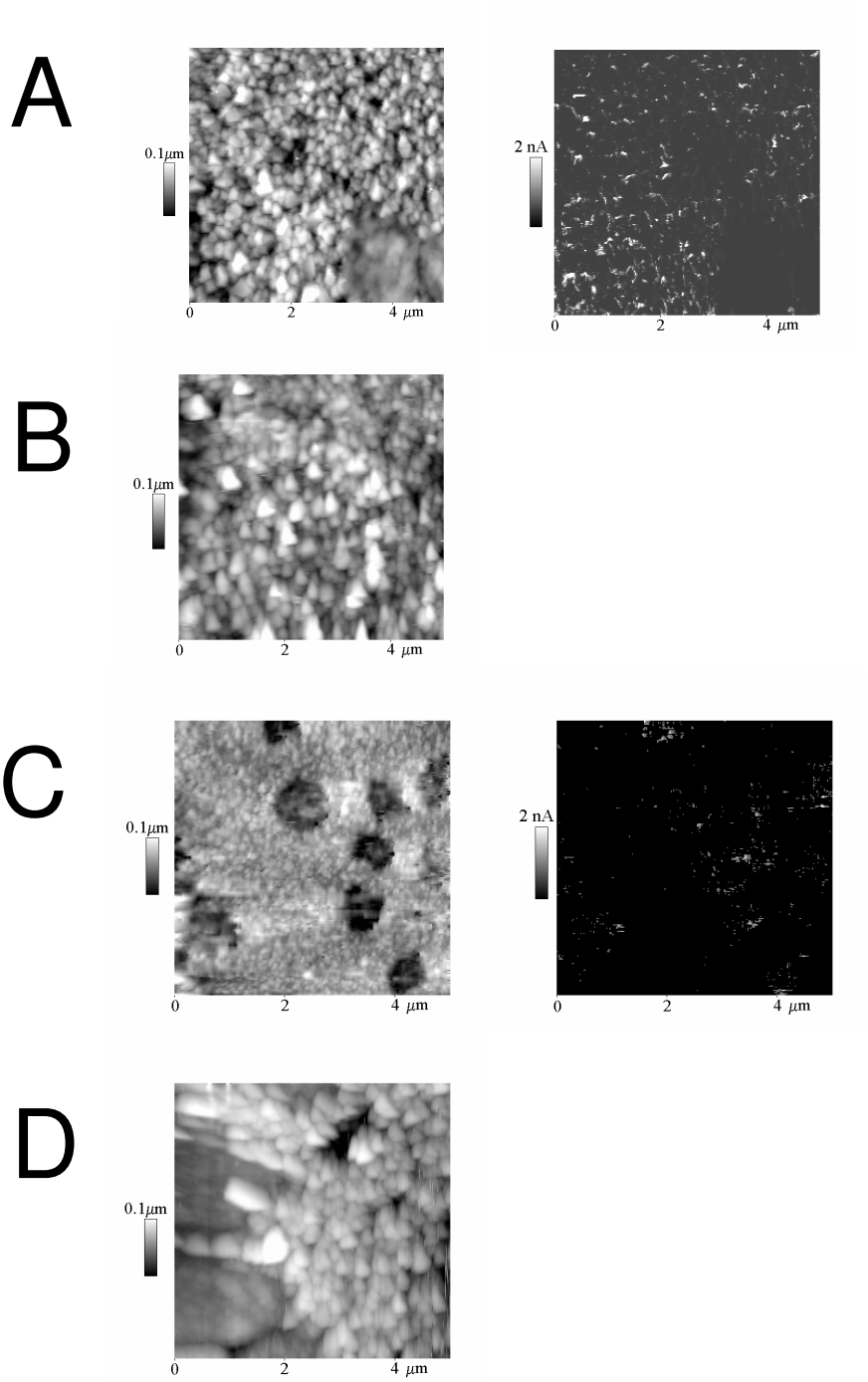

Figure 3 CSAFM topographic (left) and conductance (right) images of $LiMn_2O_4$ electrodes which were exposed to DMC and the electrolyte solution at elevated temperatures for 1 day. (A) DMC at 60°C, (B) DMC at 70°C (C) electrolyte solution at 60°C (D) electrolyte solution at 70°C. Bright areas on the conductance image represent high conductivity locations.

shallower compared to the electrode stored at 60°C. Deep cracks in the $LiMn_2O_4$ film are also visible.

Figure 4 shows Raman and SER spectra of the fresh thin-film $LiMn_2O_4$ electrode, along with electrodes which were stored in pure DMC and in the electrolyte solution at 70°C. A regular Raman spectrum of the fresh $LiMn_2O_4$ electrode consists of a series of broad bands between 300 and 700 cm^{-1}. The peaks at 624, 580 and 480 cm^{-1} are assigned to A_{1g}, $T_{2g}(3)$ and $T_{2g}(2)$ phonons. The spectrum appears nearly identical to bulk-phase

commercial $LiMn_2O_4$ powders available from chemicals suppliers.

When the $LiMn_2O_4$ electrode was exposed to pure DMC at 70°C a new feature at 656 cm^{-1} became visible. The band at 650 cm^{-1} was observed in the Raman spectra of hausmanite Mn_3O_4 and bixbyite Mn_2O_3. Because the intensities of bands at 624, 580 cm^{-1} remained unchanged, the band at 656 cm^{-1} displays clearly Mn_2O_3 character. Taking into account that the light penetration depth for $LiMn_2O_4$ is limited to 30-50 nm and the fact that there is no evidence of a Mn_2O_3 phase in the X-ray data, we postulate that only the electrode surface was enriched with Mn_2O_3 during storage in pure DMC at 70°C.

The Raman spectrum of the electrode which was stored in the electrolyte at 70°C shows even more drastic changes. The sharp peak at 624 cm^{-1} vanished, and two bands at 580 and 650 cm^{-1} dominated the spectrum. The changes observed for the Raman spectrum of the $LiMn_2O_4$ electrode stored in the electrolyte can be largely explained in terms of at least partial delithiation and conversion to λ-MnO_2. These results are fully consistent with our X-ray data.

For flat surfaces containing a thin adsorbed film, it is clear that even with an optimized system the Raman signal from the surface species will be very difficult to detect without enhancement mechanism of the Raman scattering. As a matter of fact, we could not observe any signal from the surface layer unless we sputtered a small amount of Ag nanoparticles on the electrodes. Interestingly, the SER spectra show new bands at 240, 889, 918, 985 cm^{-1}, broad multiband maxima centered around 1300 and 1600 cm^{-1}, and a series of peaks in the 2100-2160 cm^{-1} region. These new bands, except for the peak at 918 cm^{-1}, are not visible in the regular Raman spectra nor in the SER spectrum of the fresh film. Thus, they must have originated from the SEI layer. The broad band at 240 cm^{-1} can be assigned most likely to the lithium-oxygen stretch in lthium alkoxides Li-O-R (R: alkyl) and/or lihium coordinated to a carboxylic Li-(CO_2)-R or carbonate group $(Li\text{-}O)_2$-C=O. The broad peak maxima at 1300 and 1600 cm^{-1} correspond to symmetric and asymetric vibrations, respectively, of carboxyl and carbonate groups. The bands at 918 and 889, 985 are probably C-C stretch and deformation vibrations of the carboxyl groups (-COO), respectively. The complex structure of these peaks suggests clearly a

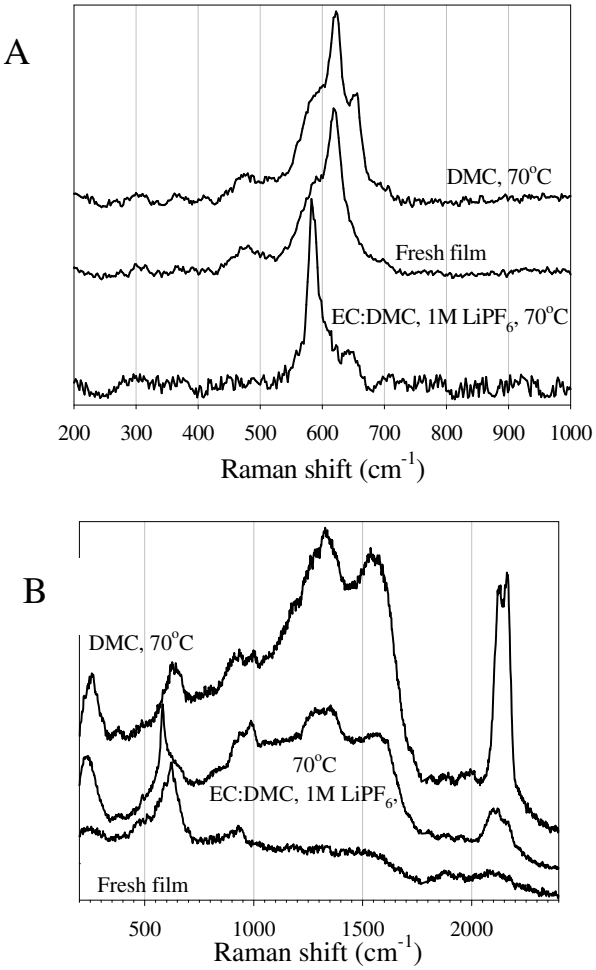

Figure 4. Regular (A) and SER spectra (B) of a fresh thin-film $LiMn_2O_4$ electrode and $LiMn_2O_4$ electrodes exposed to DMC and the electrolyte solution at 70°C for 1 day

non-uniform composition and symmetry of compounds which constitute the SEI layer. The double structure between 1300 and 1600 cm^{-1} in the SER spectra is usually attributed to surface carbonate species. Indeed, the features observed at reference Raman and SER spectra of $(COONa)_2$, HCOONa, and CH_3COOLi could not account for all the bands observed at the SER spectra of $LiMn_2O_4$ electrodes which were exposed to pure DMC and the electrolyte. The reference SER spectrum of Li_2CO_3 exhibits similar broad maxima at 1300 and 1600 cm^{-1} however it shows also sharp peaks at 1046 and 1084 cm^{-1} which are absent in the SER spectra of the SEIs. Moreover, none of the reference spectra showed such intense bands in the 2100-2160 cm^{-1} region. These features often accompany SER spectra from adsorbed molecules on silver as so-called "impurity lines". Because CO is only weakly bonded to silver at low temperatures (120 K), simple CO adsorption on silver must be ruled out. Instead, an interpretation based on stable CO-rich derived species reactively synthesized at the electrode surface from the oxygen reach SEI layer and reductive Ag particles during the sputtering seems more reasonable. The observed bands are located above and below ν_{C-O} (2135 cm^{-1}) which suggest polynuclear carbonyl complexes being responsible for the observed spectral features. However, we must point out the preliminary character of the given interpretation.

In summary, thin-film $LiMn_2O_4$ electrodes were prepared by spin coating of a precursor solution onto a Pt substrate. The electrodes have spinel structure, and they exhibited electrochemical properties similar to powder $LiMn_2O_4$ electrodes. Insulating surface layers on electrodes exposed to pure DMC or to the EC:DMC, 1M $LiPF_6$ electrolyte solution at temperatures above 60°C were detected by CSAFM and SERS measurements. It originated from DMC surface oxidation by Mn(IV). The SEI layer formation was accompanied by conversion of the original $LiMn_2O_4$ into Mn_2O_3 and λ-MnO_2 in pure DMC and the electrolyte, respectively. The surface layer formed in pure DMC at 70°C was electronically insulating and it led to complete deactivation of the electrode. A similar layer formed on the surface of the spinel electrode in the electrolyte solution, however, the electrode surface sustained serious structural damage and a large amount of manganese dissolved into the solution. Formation of the surface layer and active material loss are responsible for the observed capacity decline in this case. SER spectra showed that the surface layer contains alkoxide, carboxylic and carbonate functional groups in a complex, polymer-type structure derived from various nucleophilic reactions between $LiMn_2O_4$ and DMC and/or its intermediates

(i) Temperature-induced surface degradation of $LiNi_{0.8}Co_{0.2}O_2$ cathodes.

Figure 5 shows topographic AFM images of the cathode extracted from Cell 1 (a), and Cell 7 (b) (see Table 2) which was cycled at 70°C at 60% SOC and 3 % ΔSOC. Examination of the topographic AFM images of the cathode that was extracted from the cell cycled at 70°C (Fig. 5b) reveals a significant change in the surface morphology. The initial large and flat grains of active material are still recognizable, but the entire surface is now covered by nanocrystalline deposits. The individual particles sizes varied from 50 to 200 nm. Considerable amounts of this deposit accumulated, particularly in the inter-granular spaces, however the nanoparticles can also be found scattered randomly across the crystal planes of the active material.

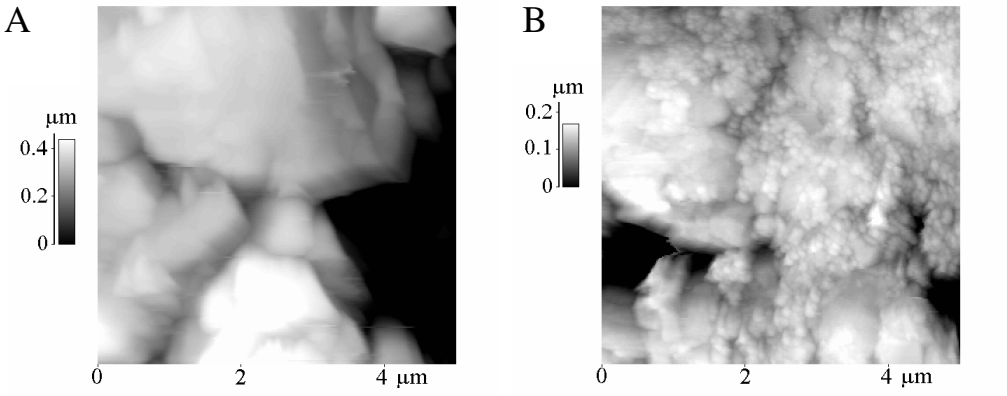

Figure 5. AFM topographic images of cathodes from the (a) Cell 1, and (b) Cell 7 (cycled at 70 ^{o}C at 60% SOC and 3 % ΔSOC)

Interestingly, we found a similar type of deposit on the surfaces of almost all cathodes from cells that were subjected to either the calendar-life or life-cycle tests. In order to quantify the AFM results and identify a clear relationship between the cathode surface morphology changes and the testing temperature, a statistical analysis of the AFM images was carried out. Figure 6 shows the surface-average and rms roughness parameters expressed versus temperature. The results at 20^{o}C correspond to the uncycled Cell no.1. It is clear from Fig. 5 that both surface roughness parameters decrease monotonically with increasing temperature. This trend is consistent with visual observations from the AFM images. The nanocrystalline deposit, which accumulated preferentially in deep cavities between the grains of active material, smoothed the surface to some extent. The decreasing gap between the surface-average and rms roughness values at higher temperatures suggests the formation of a more uniform surface with less protrusions and deep crevices. Interestingly, the smoothing effect was more pronounced in the calendar-life cells compared to the cycled cells. Such behavior suggests a precipitation mechanism of deposit formation rather than an electrochemical dissolution/redeposition process.

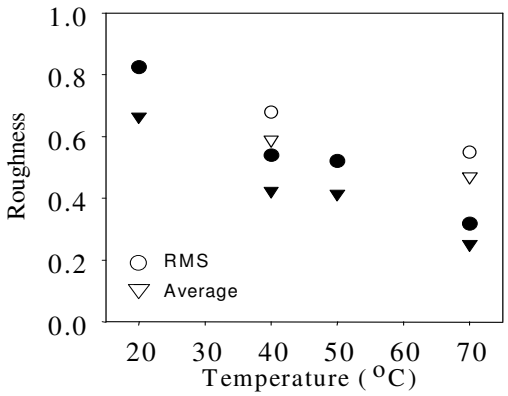

Figure 6. Surface-average and rms roughness parameters of cathodes from the virgin cell (no. 1), calendar-life cells no.2, 3, 5 (filled symbols) cycled cells no. 6 and 7 (open symbols) expressed versus temperature

To gain additional insight into the nature of the nanocrystalline deposit we studied the cathode surface with Raman spectroscopy. Figure 7 shows Raman spectra of cathodes from Cells 1 (a) and 3 (b). The Raman spectra of both cathodes are dominated by two strong and broad carbon bands at 1365 and 1580 cm^{-1} and a broad maximum centered around 500 cm^{-1}, characteristic for $LiNi_xCo_{1-x}O_2$ oxide. Close examination of the Raman bands that arise from $LiNi_xCo_{1-x}O_2$. reveals that almost all cathodes which were tested at

higher temperatures exhibit an intense peak at 558 cm^{-1}. This band, along with the band at 480 cm^{-1}, is usually associated with vibrations characteristic of Ni(III) and/or Ni(IV) oxides, and their presence can be detected in the spectrum of fresh cathodes. However, the rise of their intensities suggests selective dissolution of cobalt from the $LiNi_xCo_{1-x}O_2$ or the formation of a separate phase of nickel oxide at the cathode surface. The presence of a nanocrystalline deposit at the cathode surface supports this hypothesis. Mid-IR (wave number range 600 – 4000 cm^{-1}) data revealed no observable SEI layer on the cathode surface, which suggests the precipitate does not arise from oxidation of the electrolyte. We may assume that in the long term such phase changes combined with extensive electrode surface morphology modifications can lead to significant electrode degradation and eventual failure.

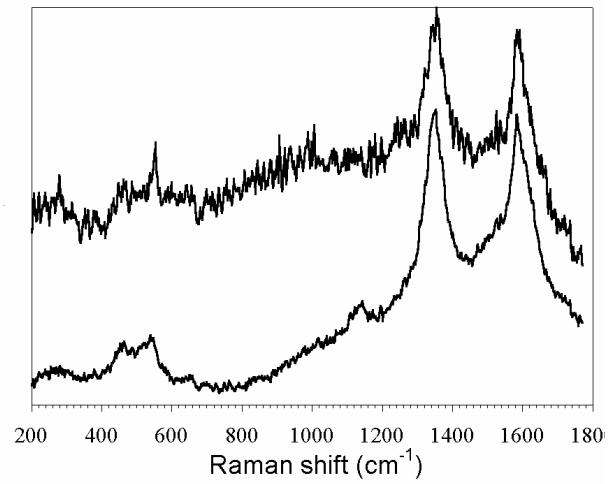

Figure 7. Raman spectra of cathodes from (a) Cell 1, and (b) Cell 3

ACKNOWLEDGMENT

This work was supported by the Director, Office of Science, Office of Basic Energy Sciences, Chemical Sciences Division; and by the Assistant Secretary for Energy Efficiency and Renewable Energy, Office of Advanced Automotive Technologies, U. S. Department of Energy, under contract number DE- AC03-76SF00098

REFERENCES

1. P. Arora, R. E. White and M. Doyle, *J. Electrochem. Soc*., **145**, 3647 (1998)
2. G. Amatucci, A. Du Pasquier, A. Blyr, T. Zhang and J.-M. Tarascon, *Electrochim. Acta,* **45**, 255 (1999)
3. R. J. Gummow, A. de Kock and M. M. Thackeray, *Solid State Ionics*, **69**, 59 (1994)
4. J. M. Tarascon, W. R. McKinon, F. Coowar, T. N. Bowmer, G. Amatucci, D. Guyomard and M. M. Thackeray, *J. Electrochem. Soc*., **141**, 1421 (1994)
5. S. J. Wen, T. J. Richardson, L. Ma, K. A. Striebel, P. N. Ross and E. J. Cairns*, J. Electrochem. Soc*., **143**, L136 (1996)
6. D. H. Jang, J. Shin and S. M. Oh, *J. Electrochem. Soc*., **143**, 2204 (1996)
7. Y. Xia, Y. Zhou and M. Yoshio, *J. Electrochem. Soc*., **144**, 2593 (1997)
8. D. H. Jang and S. M. Oh, *J. Electrochem. Soc*., **144**, 3342 (1997)
9. D. H. Jang and S. M. Oh, *Electrochim. Acta*, **43**, 1023 (1998)
10. A. Blyr, C. Sigala, G. Amatucci, D. Guyomard, Y. Chabre and J-M. Tarascon*, J. Electrochem. Soc*., **145**, 194 (1998)
11. M. M. Thackeray, Y. S-Horn, A. J. Kahaian, K. D. Kepler, E. Skinner, J. T. Vaughey and S. A. Hackney, *Electrochem. and Solid State Lett*., **1**, 7 (1998)

12. O. Shilling and J. R. Dahn, *J. Electrochem. Soc*., **144**, 2593 (1998)
13. A. Du Pasquier, A. Blyr, P. Courjal, D. Larcher, G. Amatucci, B. Gerand and J-M. Tarascon, *J. Electrochem. Soc*., **146**, 428 (1999)
14. A. Du Pasquier, A. Blyr, A. Cressent, C. Lenain, G. A. Amatucci and J. M. Tarascon, *J. Power Sources*, **81-82**, 54 (1999)
15. J. Cho and M. M. Thackeray, *J. Electrochem. Soc*., **146**, 3577 (1999)
16. H. Huang, C. A. Vincent and P. Bruce, *J. Electrochem. Soc*., **146**, 481 (1999)
17. R. Kostecki, F. Kong, Y. Matsuo and F. McLarnon, *Electrochim. Acta*, **45**, 225 (1999)
18. T. Inoue and M. Sano, *J Electrochem. Soc*., **145**, 3704 (1998)
19. G. Pistoia, A. Antonini, R. Rosati and D. Zane, *Electrochim. Acta*, **41**, 2683 (1996)
20. D. Aurbach, K. Gamolsky, B. Markovsky, G. Salitra, Y. Gofer, U. Heider, R. Oesten and M. Schmidt, *J. Electrochem.Soc*., **147**, 1322 (2000)
21. ATD test plan for ATD 18650 GEN 1 lithium ion cells, Revision 4, December 8, 1999, INEEL
22. X. Zhang, P. N. Ross, Jr., R. Kostecki, F. Kong, S. Sloop, J. B. Kerr, K. Striebel, E. J. Cairns and F. McLarnon, *J. Electrochem. Soc.,* submitted